Tellus (1995), 47A, 197–220
Printed in Belgium – all rights reserved

TELLUS
ISSN 0280–6495

Sensitivity of a general circulation model to parameterizations of cloud-turbulence interactions in the atmospheric boundary layer

By SABINE BRINKOP[1], *Meteorologisches Institut der Universität Hamburg*, and ERICH ROECKNER*, *Max-Planck-Institut für Meteorologie, Bundesstrasse 55, D-20146 Hamburg, Germany*

(Manuscript received 29 November 1993; in final form 24 May 1994)

ABSTRACT

Several approaches to parameterize the turbulent transport of momentum, heat, water vapour and cloud water for use in a general circulation model (GCM) have been tested in 1-dimensional and 3-dimensional model simulations. The schemes differ with respect to their closure assumptions (conventional eddy diffusivity model versus turbulent kinetic energy closure) and also regarding their treatment of cloud-turbulence interactions. The basic properties of these parameterizations are discussed first in relation to column simulations of a stratocumulus-topped atmospheric boundary layer (ABL) under a strong subsidence inversion during the KONTROL experiment in the North Sea. It is found that the K-models tend to decouple the cloud layer from adjacent layers above and below because the turbulent activity is calculated from local variables. The higher-order scheme performs better in this respect because internally generated turbulence can be transported up and down through the action of turbulent diffusion. Thus, the TKE-scheme provides not only a better link between the cloud and the sub-cloud layer but also between the cloud and the inversion as a result of cloud-top entrainment. In the stratocumulus case study, where the cloud is confined by a pronounced subsidence inversion, increased entrainment favours cloud dilution through enhanced evaporation of cloud droplets. In the GCM study, however, additional cloud-top entrainment supports cloud formation because indirect cloud generating processes are promoted through efficient ventilation of the ABL, such as the enhanced moisture supply by surface evaporation and the increased depth of the ABL. As a result, tropical convection is more vigorous, the hydrological cycle is intensified, the whole troposphere becomes warmer and moister in general and the cloudiness in the upper part of the ABL is increased.

1. Introduction

According to ground-based cloud observations (Warren et al., 1986, 1988), it is estimated that nearly 30 % of the Earth are covered with low-level stratus and stratocumulus clouds. Extensive areas of low-level stratiform clouds are observed in regions with suppressed convection, for example over the cold ocean currents off the west coasts of the continents or in the Arctic during summer. Due to their widespread and persistent occurrence, low-level clouds are important for the energy budget of the planet. Their influence on climate is basically twofold: First, they cool the Earth's surface by reflecting a substantial fraction of the incoming solar radiation back to space. Second, they modify the fluxes of heat, moisture and momentum at the surface and within the atmospheric boundary layer (ABL) and provide a stronger link between the ABL and the free atmosphere through enhanced turbulent entrainment which is closely related to

* Corresponding author.
[1] Present affiliation: DLR, Institut für Physik der Atmosphäre, D-82230 Weßling, Germany.

longwave radiative cooling at cloud top. Although these interactions are broadly understood from observations (e.g., Albrecht et al., 1988; Nicholls and Leighton, 1986; Nicholls and Turton, 1986), large eddy simulations (e.g., Deardorff, 1980; Moeng, 1986; Moeng and Schumann, 1991) and higher-order closure modelling (e.g., Chen and Cotton, 1987), their parameterization in general circulation models (GCMs) is still in its infancy.

First attempts of parameterizing the cloud-topped ABL for use in a GCM were made by Suarez et al. (1983) and Randall et al. (1985) on the basis of the mixed-layer approach (Lilly, 1968). Fractional cloudiness was not parameterized, however. The results show a realistic position of the marine stratocumulus cloud decks, but the mean cloud cover and frequency of occurrence are underestimated. Moreover, the model was not able to reproduce the persistent summertime Arctic stratus. A different approach on the basis of an eddy diffusivity model (K-model) was developed by Smith (1990) who modified the local Richardson number (and thus the eddy diffusion coefficient) by using "cloud-conservative" quantities such as the total cloud water content and the cloud water potential temperature instead of water vapour and potential temperature, respectively. Moreover, a statistical cloud model was used to estimate the cloud water content and the fractional cloud cover. This so-called "moist" Richardson number approach led to a significantly improved simulation of the marine stratocumulus cloud regimes in comparison to a conventional K-model. A similar formulation was tested in a one-dimensional version of the ECHAM model used in Hamburg for climate research (Roeckner et al., 1992). It was found that a conventional "dry" formulation of the Richardson number failed to reproduce the observed temperature profile in the ABL (Brinkop, 1991). The basic limitation of both schemes, however, (irrespective of a dry or a moist formulation of the Richardson number) is related to the dependence of the eddy diffusion coefficient on local buoyancy and wind shear which tends to suppress any interaction between the cloud layer and the inversion above.

In the present study, a new attempt is made to parameterize the cloud-topped ABL in a GCM by using the Prandtl-Kolmogorov formulation of the eddy diffusivity as a function of the turbulent kinetic energy (TKE). The TKE-closure, sometimes referred to as 1.5-order closure because second-order moments are simulated by a prognostic equation while the K-model is still retained, has several advantages over a conventional first order scheme. It allows, for example, to take the history of turbulence into account, and it is non-local in the sense that the TKE generated in the surface layer or in the cloud layer, for example, can be transported vertically and horizontally by turbulent diffusion and advection. Also, analogous to the "moist" first-order scheme, cloud effects on turbulent transfer are taken into account by formulating the buoyancy flux and the vertical diffusion of heat and water (all phases) in terms of cloud-conservative quantities.

In Section 2, the ABL parameterizations tested in this study are described. The basic properties of the schemes are investigated in one-column simulations on the basis of observational data for initializing and validating the models (Section 3). In Section 4 we present results of perpetual January simulations using a coarse-resolution version (T21) of the ECHAM model with the ABL formulations discussed in Section 2. Finally, the main conclusions are summarized in Section 5. We do not attempt to propose a "best" parameterization by comparing the simulated climates with observations because the conclusion would depend on the physics and the resolution of the particular model used for the study. Instead, we analyse selected terms of the heat and water budget in order to investigate the mechanisms discussed in Section 3 in a more realistic dynamical environment. The sensitivity of the simulated climate to changed formulations of ABL processes will be subject of a forthcoming study on the basis of a high-resolution GCM.

2. ABL parameterizations

All ABL parameterizations discussed below are based on the eddy diffusivity concept (K-model), i.e., the turbulent fluxes of heat, specific humidity, cloud water and momentum are parameterized in terms of the gradient of the respective variable ψ with a suitable eddy diffusion coefficent K_ψ,

$$\overline{w'\psi'} = -K_\psi \frac{\partial \psi}{\partial z}. \quad (1)$$

At the upper boundary of the model the turbulent fluxes are assumed to vanish while the surface fluxes are calculated on the basis of the Monin-Obukhov similarity theory in exactly the same way as in the ECMWF and ECHAM models (Louis, 1979). The ABL-parameterizations differ only with respect to the eddy diffusivity formulation.

2.1. *STDR: Standard scheme with dry Richardson number*

This scheme, which is used as a standard reference against which the other formulations are compared, has been developed by Louis (1979) for the ECMWF model and is now widely used in numerical weather prediction models and climate models. The eddy diffusivity (subscript $_h$) is identical for heat and humidity while eddy viscosity (subscript $_m$) is different. Both are functions of Richardson number, vertical wind shear and mixing length l,

$$K_{m,h} = l_{m,h}^2 \left| \frac{\partial V}{\partial z} \right| f_{m,h}(\mathrm{Ri}), \tag{2}$$

where l is confined by an asymptotic value (λ) as suggested by Blackadar (1962),

$$\frac{1}{l_{m,h}} = \frac{1}{\kappa z} + \frac{1}{\lambda_{m,h}}. \tag{3}$$

κ is the von Karman constant and z is height. Assuming horizontally homogenous conditions and neglecting advection, the "dry" bulk Richardson number is given by:

$$\mathrm{Ri} = \frac{g}{\theta_v} \frac{\Delta\theta_v \, \Delta z}{(\Delta u)^2 + (\Delta v)^2}. \tag{4}$$

Δ denotes the difference of the respective quantities between adjacent model levels, and θ_v is the virtual potential temperature defined in the traditional way without the liquid water term.

2.2. *STCC: Standard scheme using cloud-conservative variables*

The only difference between this scheme which is used, for example, in the most recent version of the ECHAM model (Roeckner et al., 1992), and the STDR scheme is that cloud-conservative quantities are applied in the definition of the Richardson number (Smith, 1990). The buoyancy flux is reformulated according to

$$\overline{w'\theta_v'} = A\overline{w'\theta_L'} + D\theta\overline{w'q_t'} \tag{5}$$

and includes the effect of condensation by defining a cloud water potential temperature (θ_L) and a total water content (q_t) according to Betts (1973),

$$\theta_L = \theta - \frac{L}{c_p}\frac{\theta}{T} m, \tag{6}$$

$$q_t = q + m, \tag{7}$$

where θ is potential temperature, T temperature, q specific humidity and m cloud water mixing ratio. The coefficients A and D are defined after Deardorff (1980) in unsaturated air as:

$$A = 1 + 0.61q, \qquad D = 0.61, \tag{8}$$

and in saturated air as:

$$A = (1 + 0.61q_t) - 0.622 \frac{L}{R_d T} q_s \times \frac{\left(\frac{L}{c_p T}(1 + 0.61q_t) - 1.61\right)}{\left(1 + 0.622 \frac{L^2}{R_d c_p T^2} q_s\right)}, \tag{9}$$

$$D = \frac{L}{c_p T} A - 1. \tag{10}$$

For grid points with partial cloudiness the coefficients are calculated as a weighted mean of the unsaturated and the saturated case with the fractional cloud cover as the weighting factor. A "moist" Richardson number can then be defined as

$$\mathrm{Ri} = \frac{g}{\theta_v} \frac{(A\,\Delta\theta_L + \theta D\,\Delta q_t)\,\Delta z}{(\Delta u)^2 + (\Delta v)^2}, \tag{11}$$

which replaces the dry Ri (4) while the function $f(\mathrm{Ri})$ in the definition of the eddy diffusivity (2) remains unchanged.

2.3. *TKAD: Turbulent kinetic energy closure including TKE-advection*

For a more realistic representation of the cloud-topped ABL, the first-order closure scheme as

described above is replaced by a 1.5-order closure scheme with the Prandtl-Kolmogorov parameterization of the eddy diffusivity in terms of the turbulent kinetic energy E,

$$K_{m,h} = l'_{m,h} c_1 \sqrt{E}, \tag{12}$$

where l' is the mixing length, c_1 is a constant (0.516; Mailhot and Benoit, 1982) and E is defined as $(\overline{u'^2} + \overline{v'^2} + \overline{w'^2})/2$ where u', v', w' are the turbulent fluctuations of the wind components in cartesian coordinates. The mixing length formulation (3) is modified to a include a term which reduces the length scale in the case of stable stratification (Deardorff, 1980),

$$\frac{1}{l'_{m,h}} = \frac{1}{l_{m,h}} + \frac{1}{c_2 \sqrt{E/N^2}}, \tag{13}$$

where N is the Brunt Vaisala frequency and c_2 is an empirical constant. E is calculated from the turbulent kinetic energy equation:

$$\frac{\partial E}{\partial t} = -V_i \frac{\partial E}{\partial r_i} - \frac{\partial \overline{w'E'}}{\partial z} + \frac{g}{\theta_v} \overline{w'\theta'_v}$$

$$- c_1^3 \frac{E^{3/2}}{l'_m} - \overline{u'w'} \frac{\partial u}{\partial z} - \overline{v'w'} \frac{\partial v}{\partial z}, \tag{14}$$

where the 1st term on the right-hand side denotes advection (tensor notation), the 2nd the turbulent vertical transport of E, the 3rd production/destruction of E by buoyancy, the 4th dissipation, and finally the production of E by wind shear. All turbulent fluxes are calculated from K-theory with K according to (12), and the buoyancy flux is defined by (5). The numerical technique to solve the TKE equation is discussed in Appendix A.

The scheme described above (TKAD) is the most complete one used in this study. It includes the advection in the TKE equation and uses also cloud-conservative variables. In a series of GCM experiments (cf., Section 4) the relevance of these processes is investigated: The scheme TKCC, for example, does not include the TKE advection while the cloud-conservative quantities are retained. TKDR is a "dry" TKE-scheme analogous to the "dry" first-order scheme STDR. Moreover, we test the sensitivity of the parameter c_2, hereafter called entrainment parameter due to its impact on mixing length (13) and eddy diffusivity in the inversion layer particularly. At the extremes, turbulent entrainment of relatively dry and warm air from the inversion layer into the ABL will be completely suppressed in the case of vanishing c_2 and attain its maximum rate if c_2 approaches infinity. The actual value used in this study ($c_2 = 0.4$) was obtained from a series of one-column model simulations (Brinkop, 1992) of a cloud-topped ABL over the North Sea and in the Arctic (Brümmer, 1986; Finger and Wendling, 1990) and of day 33 of the Wangara experiment (Clarke et al., 1971) characteristic of a cloud-free ABL. Since this parameter is the most uncertain one in the TKE-scheme, two additional experiments were performed with a doubled entrainment parameter (TKDE) and a halved one (TKHE), respectively.

Table 1. *List of ABL parameterizations*

Scheme	Order of closure	Cloud conservative variables	TKE advection	Entrainment parameter
STDR	1	no	—	—
STCC	1	yes	—	—
TKAD	1.5	yes	yes	0.4
TKCC	1.5	yes	no	0.4
TKHE	1.5	yes	no	0.2
TKDE	1.5	yes	no	0.8
TKDR	1.5	no	no	0.4

The ABL formulations tested in this study are listed in Table 1.

3. One-column model simulations

3.1. *Model and experiments*

Before implementing the ABL parameterizations described above in the GCM, they have first been tested in a one-column version of the ECHAM model. A brief description of the basic features of the ECHAM model is given in Subsection 4.1. Here it may suffice to present the basic equations which are (except for the momentum equation not shown here) the thermodynamic equation and the budget equations for specific

humidity (q) and cloud water mixing ratio (m), respectively:

$$\frac{\partial T}{\partial t} = -\frac{\partial}{\partial z}\overline{w'T'} + (C-E)\frac{L}{c_p} + \mathrm{CV}(T) - \frac{1}{\rho c_p}\frac{\partial F}{\partial z} - V_i\frac{\partial T}{\partial r_i}, \quad (15)$$

$$\frac{\partial q}{\partial t} = -\frac{\partial}{\partial z}\overline{w'q'} - (C-E) + \mathrm{CV}(q) - V_i\frac{\partial q}{\partial r_i}, \quad (16)$$

$$\frac{\partial m}{\partial t} = -\frac{\partial}{\partial z}\overline{w'm'} + (C-P) - V_i\frac{\partial m}{\partial r_i}. \quad (17)$$

$C>0$ ($C<0$) describes the effect of condensation (evaporation) of water vapour (cloud water) and $E>0$ is the evaporation of precipitation. P represents the conversion of cloud droplets into rain drops and/or the sedimentation of ice crystals. The tendency for all convective processes is symbolized by CV, and F is the sum of the shortwave and longwave radiative flux densities. In the advection terms which may either be neglected or specified as a constant or time-dependent forcing, $V=(u, v, w)$ is the vector of the wind velocity, and r_i ($i=1, 2, 3$) are the cartesian coordinates (x, y, z). In the 1d model experiments discussed below, we only consider radiation, stratiform cloud processes, vertical diffusion, and surface fluxes. In contrast to the 3d model study (Section 4), convection and advection is not taken into account. The model has the same vertical resolution as the 3d model. There are 19 levels up to a pressure level of 10 hPa, 5 of which are placed below a height of about 1500 m with the lowest level at about 30 m representing the top of the surface layer. There is certainly a need for a better vertical resolution. Thin cloud layers, for example, are not properly resolved in the current configuration, and resolution experiments using Wangara data also show an improved simulation of the ABL depth for a threefold increase of the vertical resolution (Brinkop, 1992).

The column model is initialized with vertical profiles of temperature, specific humidity and wind measured by the FALCON-20 aircraft on 16 October 1985, between 12.30 and 13.30 local time during the KONTROL campaign in the southeast part of the North Sea (Brümmer, 1986). The large-scale circulation was dominated by a persistent warm anticyclone over the British Isles with sinking motion at its eastern flank. An extended and persistent stratocumulus field covered the south and east part of the North Sea, North Germany, The Netherlands and Belgium. At the measurement site, the ABL had its largest extent of about 800 m in the afternoon with a stratocumulus deck of nearly 600 m thickness underneath. The temperature lapse rate below cloud base was close to neutral, it was moist adiabatic inside the cloud and there was a strong inversion with a temperature jump of 5.5 K above cloud top and a specific humidity jump of about 1.5 g/kg. The sea surface temperature was about 14°C and the surface layer was slightly unstable with an air-sea temperature difference of −1°C. Additional measurements of the surface heat fluxes taken near the island of Helgoland and turbulent moisture fluxes are used for validating the simulations. Unfortunately, cloud water content and precipitation were not measured, but rainfall was reported in the experimental area. After a simulated time of about 2.5 h, a quasi-steady state was reached characterized by vanishing tendencies of the prognostic variables and adaptation of the turbulence quantities to the vertical profiles of temperature, humidity and cloud water (Brinkop, 1992). The wind profile was kept constant during the integrations.

3.2. *Results*

Table 2 shows a comparison of observed and simulated parameters for the stratocumulus case study during the KONTROL campaign in the North Sea. While the schemes using cloud-conservative variables (STCC and TKCC) are able to reproduce the observed surface fluxes and the moist adiabatic lapse rate in the cloud layer to a reasonable degree, the latent heat flux in the STDR model is substantially smaller than in STCC and TKCC, and it is smaller by 6 W/m^2 than the observations suggest, although this difference may not be significant considering the uncertainties of the measurements and the sampling problem, in particular. Moreover, the ABL in STDR is relatively cold and moist (in terms of relative humidity) with a near-neutral lapse rate throughout the cloud layer, and this model generates a second cloud layer just above the surface layer, a feature which

Table 2. *Comparison of observed and simulated parameters of a stratocumulus case study in the North Sea (see text)*

	SH (W/m^2)	LH (W/m^2)	m (g/kg)	γ (°C/100 m)	$\overline{w'q'}$ (m/s)	K_h (m^2/s)
Obs	10	50	—	~0.3	~0.01	—
STDR	12	44	0.19	0.09	0.0001	0.04
STCC	13	53	0.25	0.25	0.0003	0.08
TKCC	11	53	0.21	0.21	0.004	1.37

The differences between the ABL schemes are sketched in Table 1. SH and LH are the sensible and latent surface heat fluxes, respectively, m is the cloud water mixing ratio (here: liquid phase only), $\gamma = \partial\theta/\partial z$ denotes the potential temperature lapse rate in the cloud layer, $(w'q')$ the turbulent vertical humidity flux at cloud top and K_h is the eddy diffusivity.

was neither observed nor simulated by any other scheme. All models underestimate the turbulent moisture flux into the inversion layer above cloud top. Nevertheless, there is a substantial difference between the TKCC-scheme which simulates about 40% of the observed flux and the first-order closure schemes which simulate only 1 and 3% of the observed flux, respectively. The reasons for these differences in the simulated turbulent moisture fluxes at cloud top are related to the different treatment of cloud top entrainment. In STDR and STCC, due to the dependency of the eddy diffusivity on local parameters only, the turbulence in the stable regime above the cloud layer is shut down completely (note the near-zero value of K_h). In the TKCC-experiment, on the other hand, the turbulent kinetic energy generated by buoyancy in the cloud layer is transported upward and downward by vertical diffusion so that a small but non-negligible level of turbulence is maintained even in the inversion layer. This turbulent entrainment of relatively warm and dry air from the inversion into the cloud layer results in a slightly smaller cloud water content as compared to STCC.

The sensitivity of the TKE-scheme to the choice of the entrainment parameter is demonstrated in Table 3. Doubling (halving) the parameter leads to a warmer (colder) ABL with reduced (increased) sensible heat fluxes at the surface, while the latent heat fluxes change in the opposite sense. Hence, the entrainment of relatively warm and dry air into the ABL tends to reduce the Bowen ratio. As to be expected from the results shown in Table 2, increased entrainment enhances the evaporation of cloud water with a corresponding effect on the reflection of solar radiation.

According to Table 4, the models STCC and TKCC show a different sensitivity to the initial moisture content in the inversion layer. As discussed above, the STCC and STDR models tend to decouple the cloud layer from the stable layer above, so that these models are essentially independent of the state of the free atmosphere. The TKCC model on the other hand, due to the vertical diffusion of turbulent kinetic energy, allows an

Table 3. *As Table 2, except for the sensitivity of the TKE-scheme to halving and doubling the entrainment parameter, respectively*

	SH (W/m^2)	LH (W/m^2)	m (g/kg)	SW (TOA)$^\uparrow$ (W/m^2)	SW (SFC)$^\downarrow$ (W/m^2)
TKHE	12	52	0.24	336	142
TKCC	11	53	0.21	330	149
TKDE	9	53	0.19	318	164

SW (TOA)$^\uparrow$ denotes the top-of-atmosphere reflected solar radiation, and SW (SFC)$^\downarrow$ is the downward solar radiation at the surface.

Table 4. *As Table 3, except for the sensitivity of the STCC and TKCC schemes to initial conditions*

	SH (W/m^2)	LH (W/m^2)	m (g/kg)	SW (TOA)$^{\uparrow}$ (W/m^2)	SW (SFC)$^{\downarrow}$ (W/m^2)
STCC					
initial dry	13	54	0.25	341	138
control	13	53	0.25	343	134
initial wet	12	52	0.24	336	138
TKCC					
initial dry	11	57	0.17	320	165
control	11	53	0.21	330	149
initial wet	11	51	0.22	329	147

In the "initial dry" case, the specific humidity in the inversion layer is decreased initially from 6 g/kg in the control case to 4 g/kg, while it is increased to 8 g/kg in the "initial wet" case.

interaction which crucially depends on the choice of the entrainment parameter through its influence on the mixing length under stable conditions (cf., eq. (13) and Table 3). In this particular case, an extremely dry inversion layer leads to a substantial increase of the latent heat flux at the surface and at cloud top (not shown) and to a dilution of the cloud layer with a corresponding change of the solar radiative flux at the top of the atmosphere and at the surface (Table 4, bottom).

4. Three-dimensional model simulations

4.1. Model, experiments and method of analysis

The ABL parameterizations studied in the previous section have also been implemented in the global atmospheric general circulation model ECHAM (Roeckner et al., 1992). The prognostic variables of the model are vorticity, divergence, temperature, surface pressure and the mixing ratio of water vapour and cloud water, respectively. The model equations are solved on 19 vertical levels in a hybrid pressure-sigma system by using the spectral transform method with triangular truncation at wavenumber 21 (T21). Nonlinear terms and physical processes are evaluated at grid-points of a "Gaussian grid" providing a nominal resolution of 5.625° in latitude and longitude. In the present study, however, we use a semi-Lagrangian technique (Rasch and Williamson, 1990) for computing the advection of positive definite quantities such as water vapour and cloud water. A second-order horizontal diffusion scheme is applied to vorticity, divergence and temperature beyond a threshold wavenumber $n = 15$. No horizontal diffusion is required for those variables that are treated with the semi-Lagrangian technique, i.e., water vapour and cloud water. The model physics (including the ABL-scheme "STCC", cf., Section 2 and Table 1) is identical to that applied in the most recent model version ECHAM3:

The radiation scheme uses a broad-band formulation of the radiative transfer equations with 6 spectral intervals in the terrestrial infrared and 4 intervals in the solar part of the spectrum (Hense et al., 1982). Gaseous absorption due to water vapour, carbon dioxide and ozone is taken into account as well as scattering and absorption due to aerosol and cloud. The cloud optical properties are parameterized in terms of the simulated cloud water content (Stephens, 1978). The turbulent transfer of momentum, heat, water vapour and cloud water is based upon the Monin-Obukhov similarity theory for the surface layer and the eddy diffusivity approach above the surface layer (Louis, 1979). The drag and heat transfer coefficients depend on roughness length and Richardson number, and the eddy diffusion coefficients depend on wind shear, mixing length and Richardson number in the standard ECHAM model (cf., eq. (2)) and on the turbulent kinetic energy in the experimental version of the model (cf., eq. (12)). The convection scheme comprises the effect of deep, shallow and mid-level convection on the budgets of heat, water vapour and momentum (Tiedtke, 1989). Cumulus clouds are

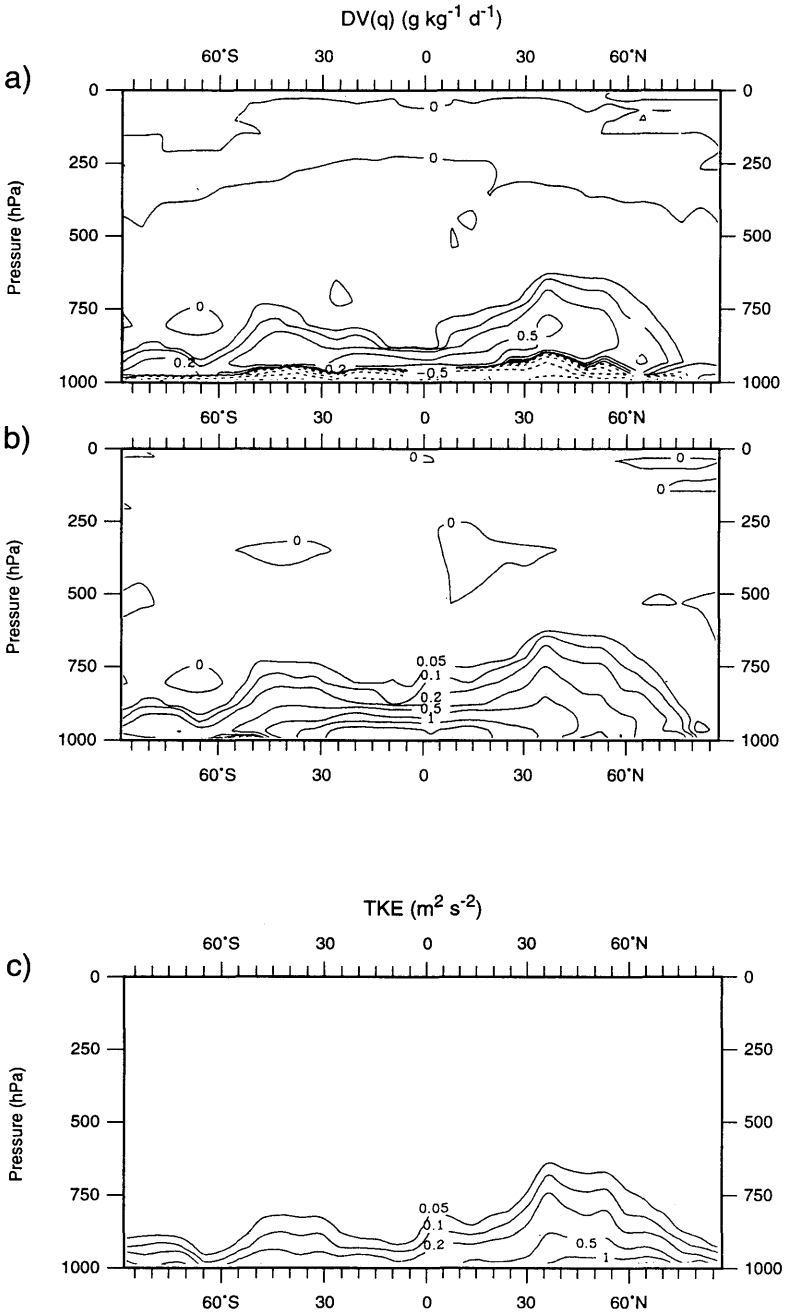

Fig. 1. Latitude-pressure cross sections of moistening due to vertical diffusion of specific humidity (upper and middle panels) and turbulent kinetic energy (lower panel). (a) Difference between experiments TKCC and STDR. Isolines (dashed for negative values): ± 0, 0.05, 0.1, 0.2, 0.5, 1, 2 (g kg^{-1} d^{-1}). (b) Experiment TKCC. Isolines: 0, 0.05, 0.1, 0.2, 0.5, 1, 2, 4, 8 (g kg^{-1} d^{-1}). (c) Turbulent kinetic energy as simulated in experiment TKCC. Isolines: 0.05, 0.1, 0.2, 0.5, 1, 2, 4 (m^2 s^{-2}).

represented by a bulk model including the effect of entrainment and detrainment on the updraft and downdraft convective mass fluxes. Stratiform clouds are calculated through a cloud water budget equation (both phases) including sources and sinks due to condensation, evaporation and precipitation formation by coalescence of cloud droplets (Sundqvist, 1978) and sedimentation of ice crystals (Roeckner et al., 1991). Sub-grid scale condensation and cloud formation is taken into account by specifying appropriate thresholds of relative humidity depending on height and static stability, and the fractional cloud cover in a grid-box is a linear function of the relative humidity. The soil model comprises the budgets of heat and water in the soil, the snow pack over land and the heat budget of permanent land ice and sea ice. The heat transfer equation is solved in a five-layer model assuming vanishing heat flux at the bottom. Vegetation effects such as the interception of rain and snow in the canopy and the stomatal control of evapotranspiration are parameterized in a highly idealized way. The runoff scheme is based on catchment considerations and takes into account sub-grid scale variations of field capacity over inhomogeneous terrain (Dümenil and Todini, 1992).

The model is run in the so-called perpetual mode with climatological sea surface temperatures and solar irradiance representative for the month of January. The diurnal variation of the sun is retained, however. The simulated time is six months in each experiment, and the results are presented as an average over the last three months, respectively. A list of the model experiments is shown in Table 1.

A change of a parameterization may eventually result in a slightly changed atmospheric state. In

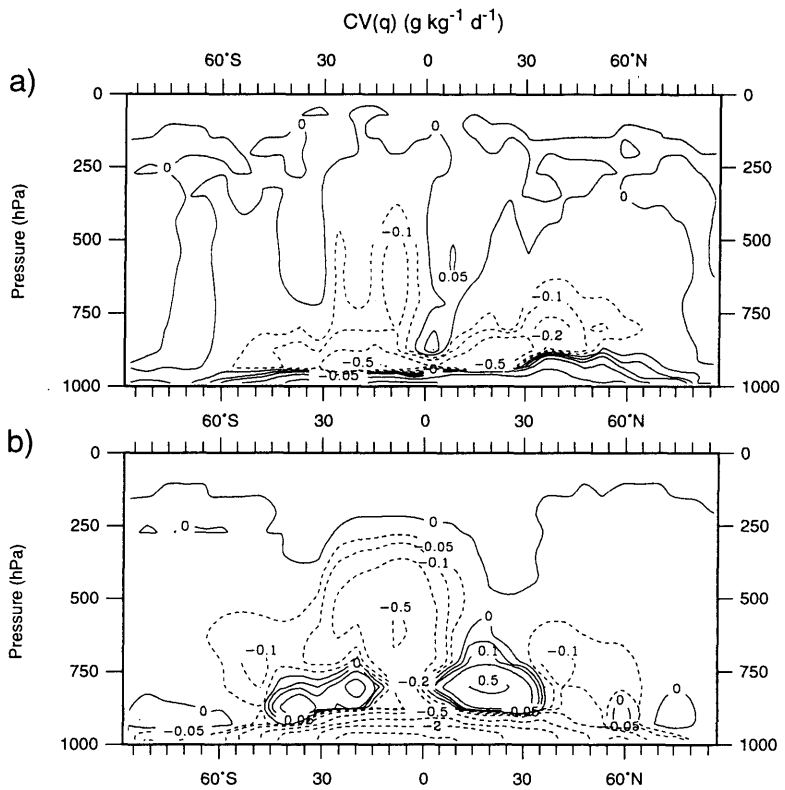

Fig. 2. As Fig. 1 except for convective moistening. (a) Difference between experiments TKCC and STDR. Isolines: ± 0, 0.05, 0.1, 0.2, 0.5, 1, 2 (g kg^{-1} d^{-1}). (b) Experiment TKCC. Isolines: ± 0, 0.05, 0.1, 0.2, 0.5, 1, 2, 4, 8 (g kg^{-1} d^{-1}).

addition to documenting this change, it may be worthwhile to analyse the contribution of the individual physical processes which govern the change. The budget equations for heat ($c_p T$), water vapour (q) and cloud water (m) which are analysed in this study are symbolically written as follows:

$$\frac{\partial T}{\partial t} = A(T) + \mathrm{DH}(T) + \mathrm{DV}(T) + \mathrm{CV}(T) + \frac{L}{c_p}(C - E) + \mathrm{RAD}(T), \quad (18)$$

$$\frac{\partial q}{\partial t} = A(q) + \mathrm{DV}(q) + \mathrm{CV}(q) - C(q) + E(m) + E(\mathrm{Pr}), \quad (19)$$

$$\frac{\partial m}{\partial t} = A(m) + \mathrm{DV}(m) + C(q) - E(m) - P(m), \quad (20)$$

with the following notation:

A: horizontal and vertical advection, including the adiabatic term in the thermodynamic equation and a conservation fix of q and m which balances the spurious loss or gain of mass associated with semi-Lagrangian advection (Rasch and Williamson, 1990).
DH: horizontal diffusion (heat only).
DV: vertical turbulent diffusion.
CV: net convective tendency due to the transport of water vapour and cloud water in convective updrafts and downdrafts, condensation, evaporation, entrainment

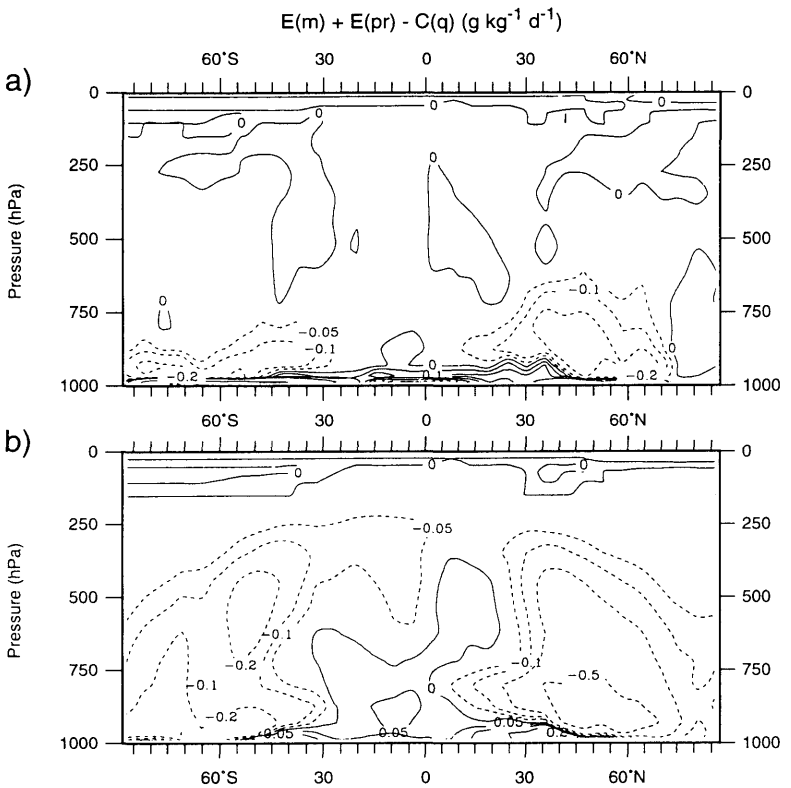

Fig. 3. As Fig. 1 except for the net phase change due to evaporation (of cloud water and precipitation) and condensation. (a) Difference between experiments TKCC and STDR. (b) Experiment TKCC. Isolines: ± 0, 0.05, 0.1, 0.2, 0.5, 1 (g kg^{-1} d^{-1}).

and detrainment, alternatively for deep, shallow and mid-level convection. There is no explicit treatment of convectively generated cloud water in the stratiform cloud scheme.

$C(q)$: condensation of water vapour in stratiform clouds.

$E(m)$: evaporation of stratiform cloud water.

$E(\mathrm{Pr})$: evaporation of stratiform precipitation in unsaturated air.

$P(m)$: stratiform precipitation rate due to coalescence processes in warm clouds and sedimentation of ice crystals in cold clouds.

RAD: temperature change due to emission and absorption of shortwave and longwave radiation. The respective SW and LW components are further decomposed into a clear-sky contribution and the cloud-radiative forcing (SW CRF and LW CRF; Ramanathan et al. 1989).

4.2. *Results*

4.2.1. Comparison between TKCC and STDR. Most of the results are presented as time-mean, latitude-height cross sections of individual terms of the water vapour budget equation. The tendency $\mathrm{DV}(q)$ due to the vertical turbulent flux divergence of q is shown in Fig. 1b for the TKCC experiment (cf., Table 1). As to be expected, the moistening of the ABL is largely controlled by surface temperature (maximum in the low-latitude surface layer) but also by the TKE distribution (Fig. 1c) which is largest in the mid-latitudinal winter hemisphere due to TKE generation by buoyancy and wind shear over the oceans in particular. The ABL height is relatively large also in

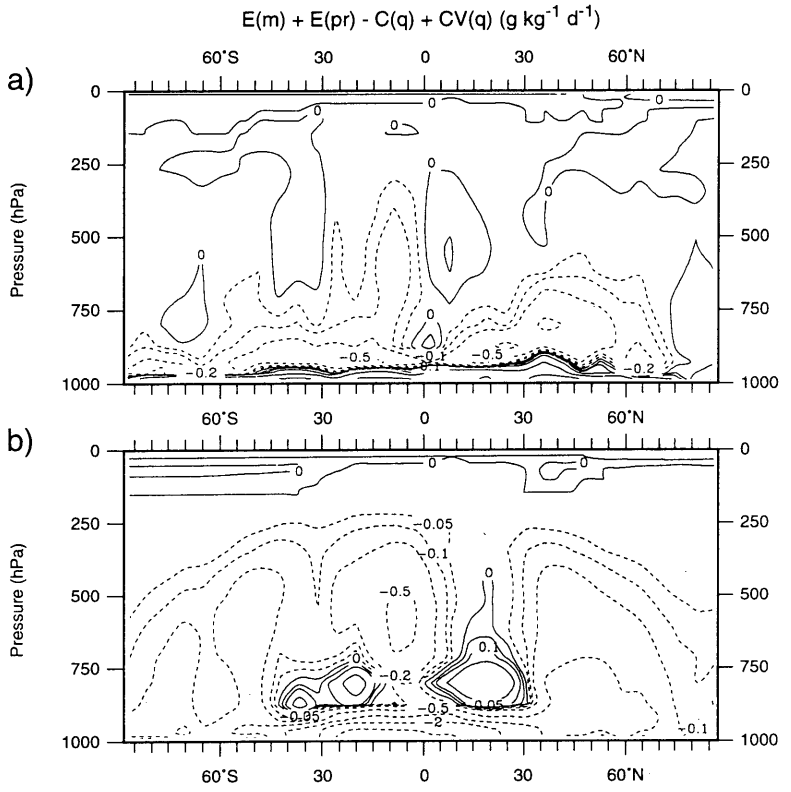

Fig. 4. Sum of all convective and stratiform phase changes shown in Figs. 2, 3. (a) Difference between experiments TKCC and STDR. Isolines: ± 0, 0.05, 0.1, 0.2, 0.5 (g kg^{-1} d^{-1}). (b) Experiment TKCC. Isolines: ± 0, 0.05, 0.1, 0.2, 0.5, 1, 2, 4, 8 (g kg^{-1} d^{-1}).

regions where either buoyant production prevails (ITCZ) or shear generation ("roaring fourties" in the Southern Hemisphere or Antarctica).

The difference between the TKCC scheme and the standard scheme STDR is shown in Fig. 1a. Relative to STDR, the TKCC scheme tends to dry the lower ABL and moisten the upper part. Ignoring a significant change of surface evaporation for the time being, this pattern is consistent with a deeper ABL maintained through processes which are ignored in STDR such as the vertical turbulent transport of TKE generated mostly in the surface layer and in the cloud layer (due to longwave radiative cooling), but also by the use of cloud-conservative quantities for calculating the buoyancy flux (cf., Section 2).

While vertical diffusion is the major source of moisture, the ABL is ventilated most efficiently by deep and shallow convection (Fig. 2b). Convection is also a net sink of moisture in those regions of the free atmosphere where convective condensation and precipitation formation prevails (tropics, mid-latitudes), while net moistening is provided by moisture exchange through shallow nonprecipitating cumulus clouds in the subtropics preferentially. There is also a net moistening through anvil detrainment in the tropical upper troposphere.

To a large extent, the difference pattern of CV (TKCC-STDR) shown in Fig. 2a is a mirror image to that shown in Fig. 1a. In the surface layer, the diminished moistening by DV in TKCC is balanced by a smaller convective drying while more moisture is exchanged by convection between the upper part of the ABL and the free troposphere. In the subtropics, the moisture exchange through shallow cumulus clouds is partly replaced by verti-

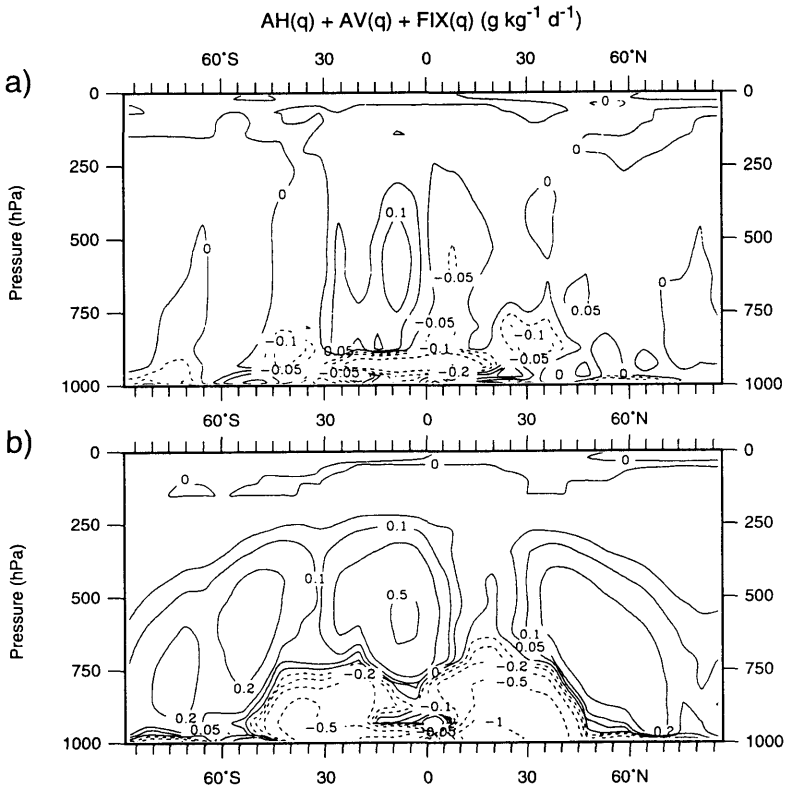

Fig. 5. As Fig. 1 except for total advection of specific humidity (horizontal + vertical + conservation fixer). (a) Difference between experiments TKCC and STDR. Isolines: ±0, 0.05, 0.1, 0.2, 0.5 (g kg^{-1} d^{-1}). (b) Experiment TKCC. Isolines: ±0, 0.05, 0.1, 0.2, 0.5, 1, 2, 4 (g kg^{-1} d^{-1}).

cal diffusion in the TKE-scheme (Figs. 1a, 2a). In the mid-latitudes of the Northern Hemisphere the negative values above about 900 hPa indicate increased convective condensation as a result of enhanced moisture transfer through vertical diffusion in the TKCC run. In the upward branch of the Hadley cell the relative convective drying is indicative of enhanced convective activity.

Fig. 3b shows the distribution of all stratiform phase changes in the TKCC simulation. Except for the lowest layers, where a net moistening by evaporation of cloud water and precipitation prevails, condensation is the dominant term, and the largest condensational drying is simulated at middle and high latitudes. The difference (TKCC-STDR) shown in Fig. 3a reveals a similar pattern and actually resembles the change of CV (Fig. 2a). When these two patterns are added together (Fig. 4a) and compared with the change of DV (Fig. 1a), it is evident that the enhanced moistening by vertical diffusion in the upper part of the ABL is compensated by drying through enhanced condensation in cumuliform and stratiform clouds. While the enhanced drying of the surface layer (Fig. 1a) is balanced by reduced convective ventilation, there is no counterpart so far for the net convective drying in the tropical middle troposphere (Fig. 4a). According to Fig. 5, however, the condensational drying of the free troposphere is balanced by the dynamics, i.e., by advective transport of moisture. The final outcome (Fig. 6a) is a general moistening of the ABL and the main troposphere in the TKCC-scheme as compared to the standard scheme STDR, except for the low-latitude surface layer and a few tropospheric regions where enhanced downward

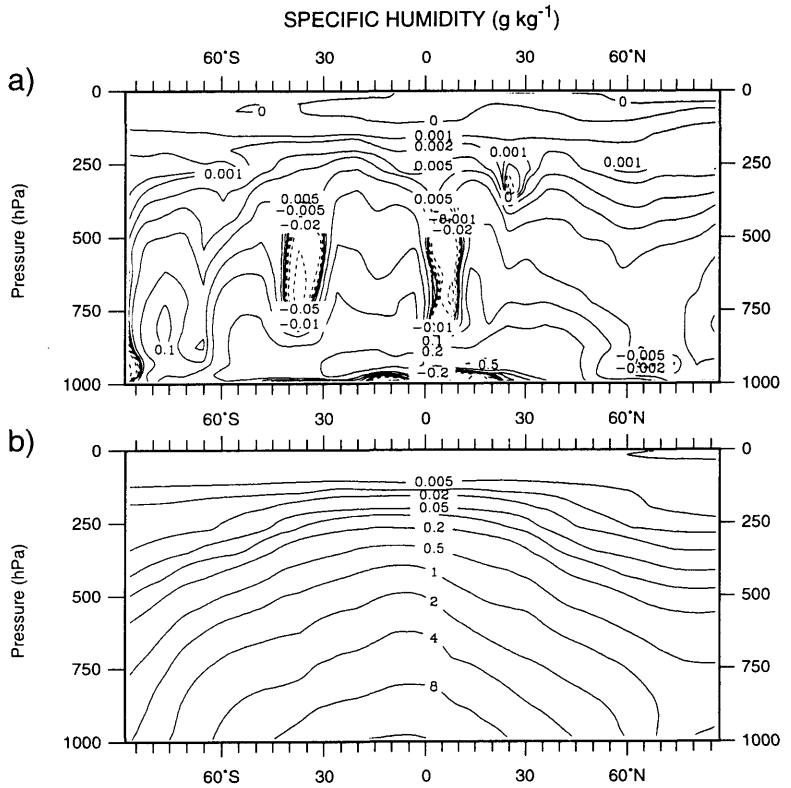

Fig. 6. As Fig. 1 except for specific humidity. (a) Difference between experiments TKCC and STDR. Isolines: ±0, 0.001, 0.002, 0.005, 0.01, 0.02, 0.05, 0.1, 0.2, 0.5, 1, 2 (g kg^{-1}). (b) Experiment TKCC. Isolines: 0.002, 0.005, 0.01, 0.02, 0.05, 0.1, 0.2, 0.5, 1, 2, 4, 8, 16 (g kg^{-1}).

Tellus A/47/2-6

motion leads to a net drying. As will be seen later, the moistening goes parallel with enhanced surface evaporation and a slightly warmer troposphere.

Consistent with the changes of the humidity budget are those of the cloud water budget. Fig. 7b shows the net cloud water tendency due to condensation, evaporation of cloud water and precipitation formation in warm and cold clouds (cf., eq. (20)) in the TKCC simulation. The budget is closed by advective and diffusive transport (not shown) from the main condensational source regions in the lower troposphere to the higher levels (basically vertical advection) and to the surface layer (basically vertical diffusion). The difference pattern (TKCC-STDR) shown in Fig. 7a has a similar structure as the TKCC distribution itself (Fig. 7b), which means that the cloud formation processes are enhanced in comparison to STDR. This is also evident for the cloud water change (TKCC-STDR) shown in Fig. 8a, and this change is similar to the humidity change (Fig. 6a) with reduced cloud water in the surface layer and also in a few regions where enhanced downward motion leads to drying, and more cloud water particularly in the upper part of the ABL. As to be expected, the cloud cover (and thus the relative humidity) changes in the same sense (Fig. 9a). The lifting of the low-level clouds in the TKCC simulation results in a radiative warming of the surface layer by enhanced downward emission from cloud base, particularly in the mid-latitudinal winter hemisphere (Fig. 10b). In the tropics, on the other hand, the longwave cloud-radiative warming in the surface layer is largely balanced by a cooling through enhanced reflection of solar radiation associated with increased cloudiness (Fig. 10a).

The TKE-closure also produces a substantial change of the sensible heat flux within the ABL.

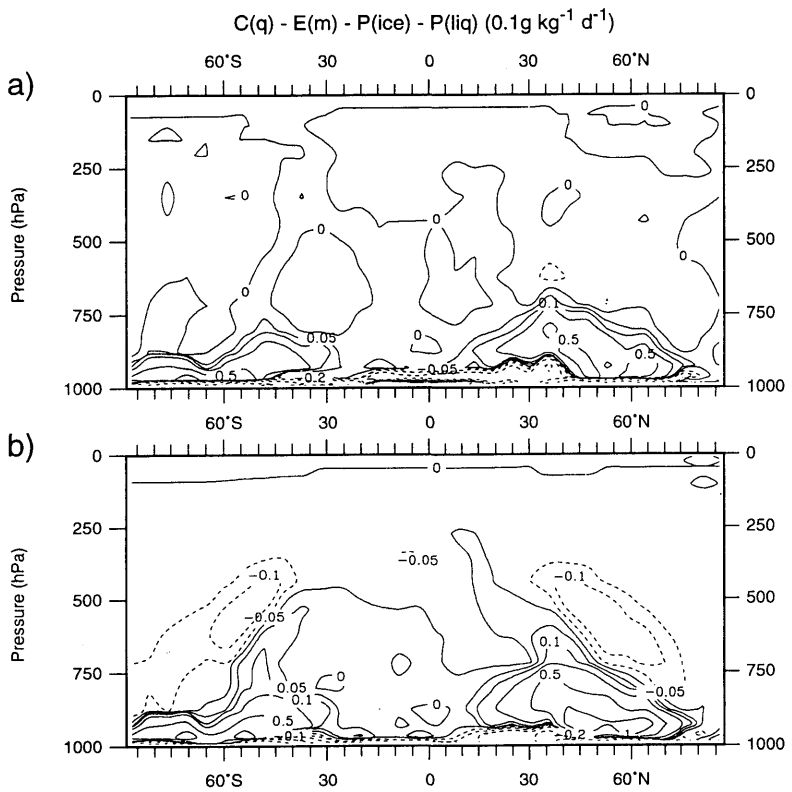

Fig. 7. Sum of all sources and sinks in the cloud water equation (condensation, evaporation and precipitation formation in cold and warm clouds). (a) Difference between experiments TKCC and STDR. (b) Experiment TKCC. Isolines: ± 0, 0.005, 0.01, 0.02, 0.05, 0.1, 0.2 (g kg^{-1} d^{-1}).

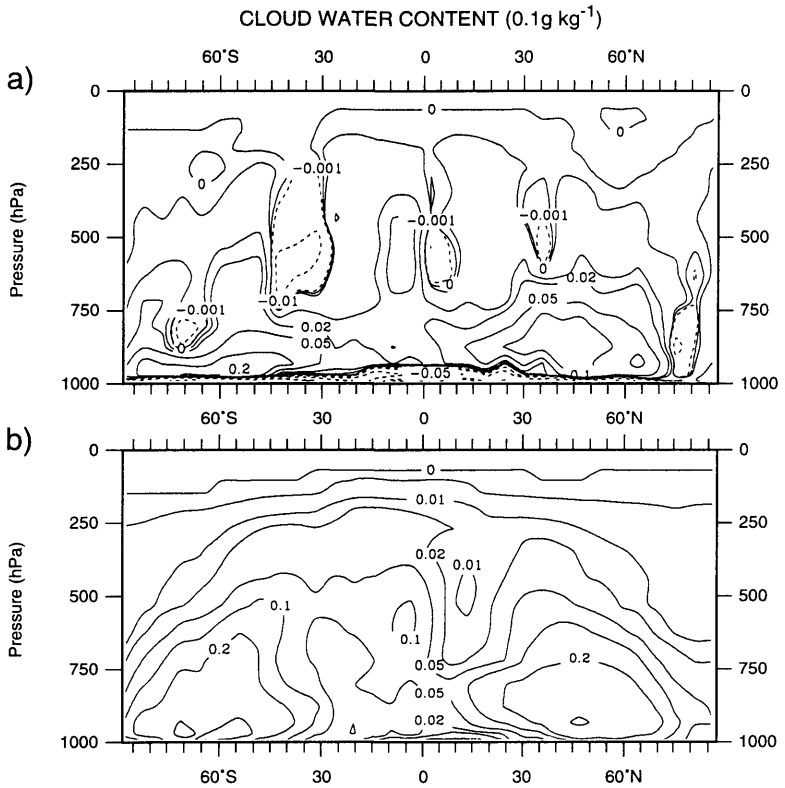

Fig. 8. Latitude-pressure cross sections of cloud water mixing ratio. (a) Difference between experiments TKCC and STDR. Isolines: ± 0, 0.0001, 0.001, 0.002, 0.005, 0.01, 0.02, 0.05 (g kg^{-1}). (b) Experiment TKCC. Isolines: 0, 0.0001, 0.001, 0.002, 0.005, 0.01, 0.02, 0.05 (g kg^{-1}).

Fig. 11 shows the respective distributions up to a height corresponding to about 735 hPa for STDR (top) and TKCC (bottom), respectively. The cooling of the upper part in the TKCC scheme results from a smaller temperature gradient (moist adiabatic lapse rate) in the upper part of the ABL (cf., Table 2) and from the higher level of turbulence maintained by vertical diffusion of TKE. In the STDR simulation the temperature gradient in the ABL is larger (close to neutral), and the sign reversal of the sensible heat flux is shifted upwards as compared to TKCC. In addition, due to the dependence of the eddy diffusion coefficient on the local Richardson number, the turbulence in the inversion layer collapses and the flux divergence vanishes.

Above the ABL, the changes of the individual components of the thermodynamic equation are relatively small, except in the tropical middle troposphere, where the convective heating maximum in the TKCC simulation is roughly 15% larger than in the STDR simulation (Fig. 12a). The stronger convective activity in TKCC (note also the enhanced convective drying, Fig. 2a) is consistent with enhanced mass transport by the Hadley cell (Fig. 13a).

4.2.2. Sensitivity experiments. In this section we discuss the sensitivity of the ABL parameterizations (cf., Table 1) to changes of various parameters and processes. Only DV(q) is presented, since this turned out to be the most sensitive term. Moreover, if a change of DV(q) is large, the changes of the other terms are large as well, and these changes occur in the same sense as discussed already in the previous section (Figs. 2–13).

One of the most uncertain parameters in the TKE formulation is the so-called entrainment parameter c_2 which determines the entrainment of

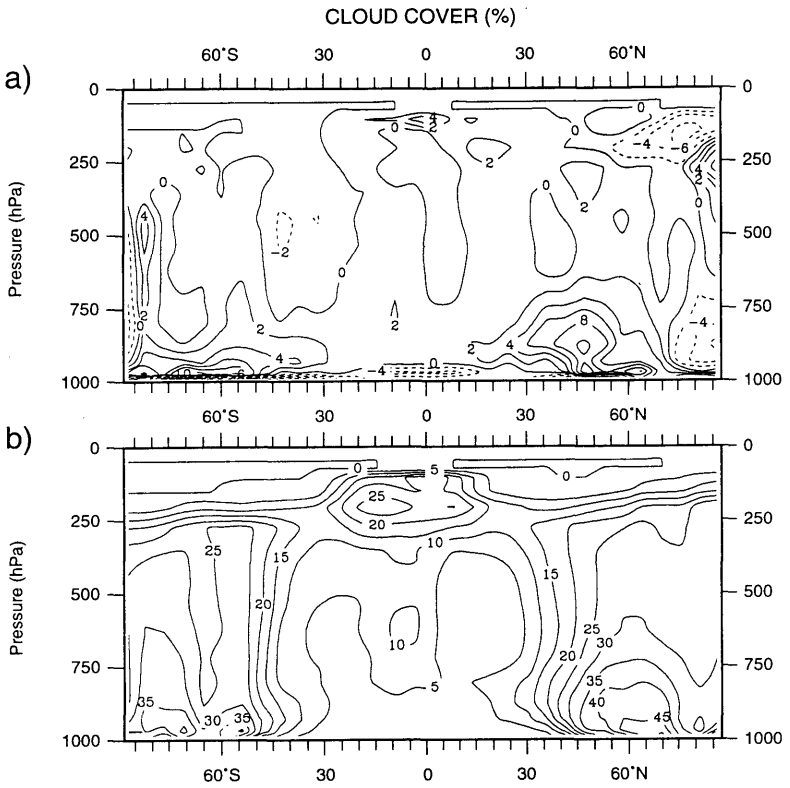

Fig. 9. As Fig. 8 except for cloud cover. (a) Difference between experiments TKCC and STDR (Contour spacing: 2%). (b) Experiment TKCC (Contour spacing: 5%).

relatively warm and dry air from the inversion layer into the ABL through its influence on the mixing length under stable conditions (cf., Sections 2 and 3). In experiment TKDE, c_2 is doubled with respect to the control experiment TKCC, while in TKHE it is halved. According to Fig. 14, a small c_2 (14a) reduces the upper ABL moistening while a large c_2 enhances the moisture transport (14b). These differences are considerably smaller, however, than those between TKCC and the standard scheme STDR (cf., Fig. 1a). Much of the difference between the latter schemes can be explained by the use of cloud conservative variables in the buoyancy flux formulation (5) of TKCC. If a "dry" formulation is used (TKDR), the change with respect to TKCC (Fig. 14c) has nearly the same magnitude as that between TKCC and STDR (Fig. 1a) with a reversed sign, of course. In a "dry" formulation both schemes tend to simulate a relatively shallow moist ABL. On the other hand, including the horizontal and vertical advection of TKE (experiment TKAD) has only a minor impact on the results (Fig. 14d).

Finally we ask whether the use of a "moist" Richardson number in the standard scheme, defined in terms of cloud-conservative quantities (10), would have a similar impact as the corresponding term in the TKE-scheme. According to Fig. 14e, however, which shows the difference between the "moist" and the "dry" formulation in the standard scheme, STCC-STDR, this difference is much smaller than that noted between TKDR and TKCC. Hence, the difference TKCC-STCC (Fig. 14f) is similar to TKCC-STDR discussed in the previous section (Fig. 1a).

The change of the surface heat budget components with respect to the "dry" standard scheme STDR is shown in Table 5. All TKE-closure

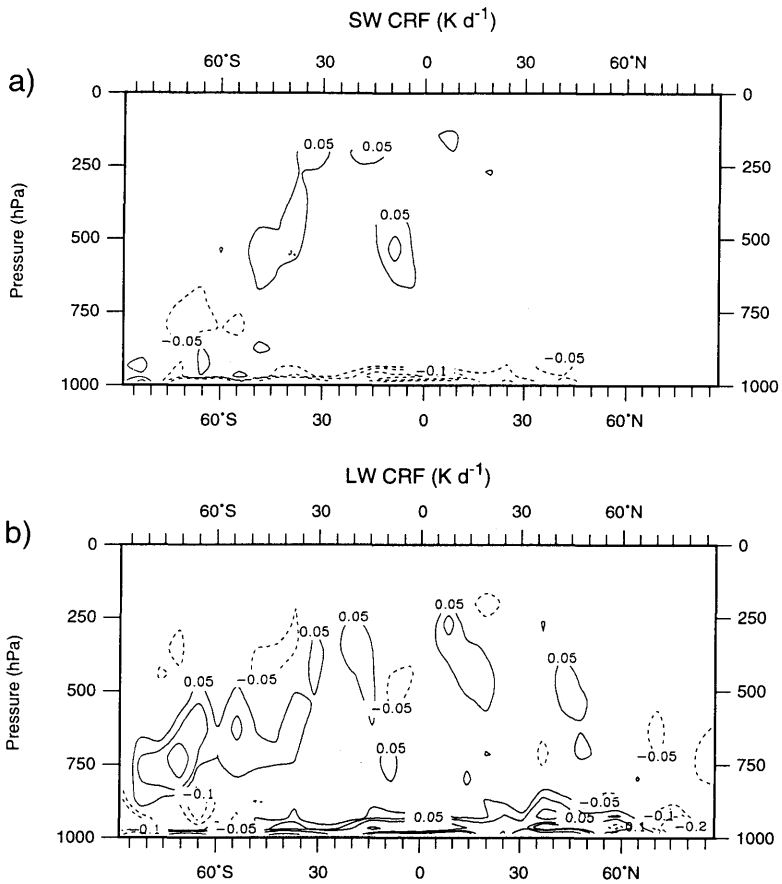

Fig. 10. Latitude-pressure cross sections of the radiative heating due to clouds. Both panels show the difference of the respective term between experiments TKCC and STDR. (a) Short-wave cloud radiative forcing. (b) Long-wave cloud radiative forcing. Isolines: ± 0, 0.05, 0.1, 0.2, 0.5, 1 (K d^{-1}).

schemes reveal a substantial decrease of the Bowen ratio with an increase of the latent heat flux at the surface by 2–6 W/m^2 and a corresponding decrease of the sensible heat flux. In the standard scheme with the "moist" Richardson number (STCC) the change is much smaller. As to be expected from DV(q) in Fig. 14, the largest change is found in the double entrainment run (TKDE) while the changes are relatively weak if the entrainment is small (TKHE) or when a "dry" buoyancy flux formulation is used in the TKE equation (TKDR). The reduced absorption of solar radiation at the surface in all experiments is caused by increased cloudiness (cf., Figs. 8a, 9a) and again this change is particularly large in the TKDE simulation. The impact on the longwave radiation budget is comparatively small in all experiments. Note that the changes do not add to zero because the sea surface temperature is prescribed.

The results of the GCM experiments seem not to be consistent with those of the column model. In the column model study (cf., Subsection 3.2) the dominant effect of the TKE closure is evaporative cloud dilution through cloud-top entrainment. In the GCM, on the other hand, cloud generating processes are favoured such as additional moisture supply through enhanced surface evaporation and lifting of ABL height. This different behaviour is probably related to the fact that in the column model study an extremely strong inversion inhibits

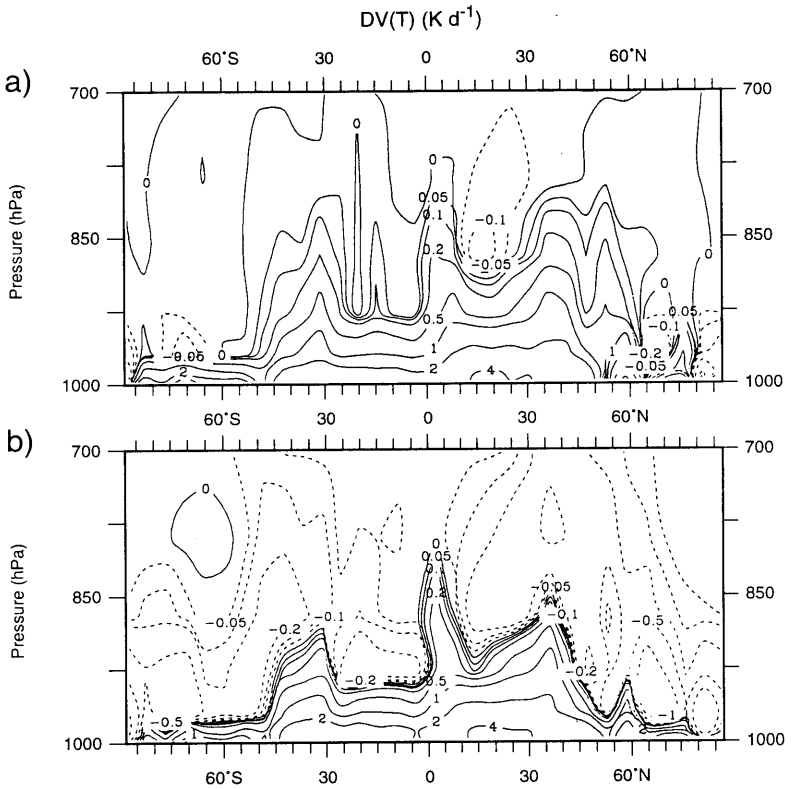

Fig. 11. Latitude-pressure cross sections of the heating due to vertical diffusion in the 5 lowest layers of the model atmosphere. (a) Experiment STDR. (b) Experiment TKCC. Isolines: ± 0, 0.05, 0.1, 0.2, 0.5, 1, 2, 4, 8 (K d^{-1}).

Table 5. *Change of the global mean surface energy budget (W/m^2) with respect to the reference experiment STDR (see Table 1)*

	ΔSH	ΔLH	ΔSW	ΔLW	ΔNET
STCC	1.2	−0.4	−0.2	−0.1	0.5
TKHE	3.8	−2.0	−0.5	−0.5	0.8
TKCC	6.7	−5.0	−1.7	−0.1	−0.1
TKDE	8.7	−6.1	−3.8	0.9	−0.3
TKAD	6.2	−4.7	−1.5	−0.1	−0.1
TKDR	3.3	−2.9	−0.2	0.1	0.3

SH and LH are the sensible and latent heat fluxes, respectively, while SW and LW are the net shortwave and longwave radiative fluxes, respectively. A positive (negative) value denotes a warming (cooling) of the surface due to the change of respective flux.

any vertical growth of the cloud, whereas in the GCM the increased coupling between the ABL and the free troposphere results in a lifting of ABL height and enhanced cloud formation in its upper part in a climatological mean sense. One should also note that the GCM allows for full dynamical interaction while in the column model the wind profile is prescribed.

5. Summary and conclusions

Several approaches to parameterize the turbulent transport of momentum, heat, water vapour and cloud water on the basis of the eddy diffusivity concept have been tested in 1d and 3d

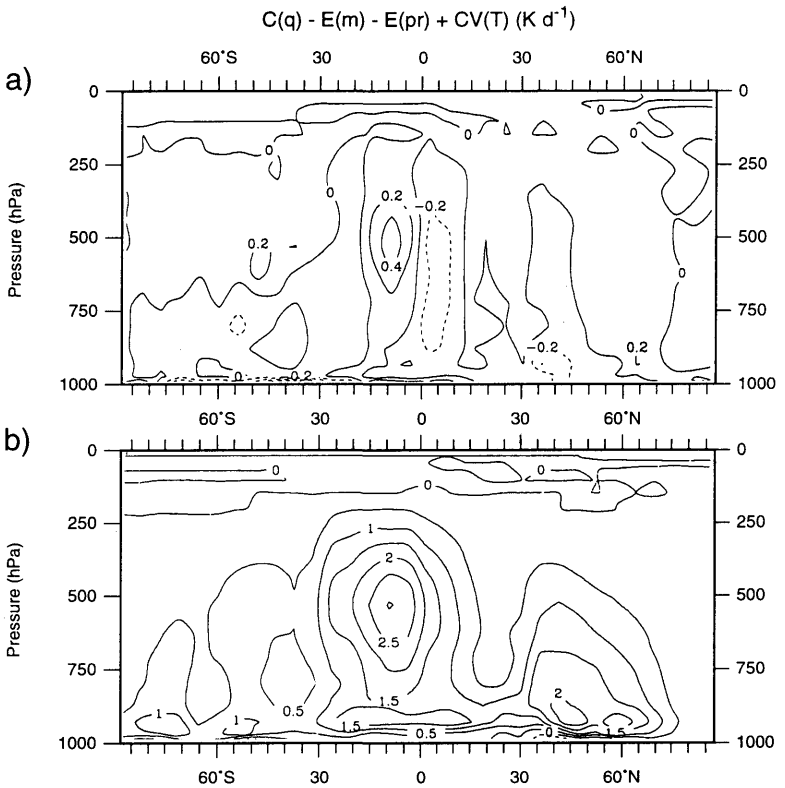

Fig. 12. Latitude-pressure cross sections of the heating due to the sum of all stratiform phase changes and convection. (a) Difference between TKCC and STDR (Contour spacing: 0.2 K d^{-1}). (b) Experiment TKCC (Contour spacing: 0.5 K d^{-1}).

model simulations. The schemes differ with respect to their order (conventional K-model versus TKE-closure) and also regarding their treatment of cloud-turbulence interactions. The results obtained from a case study of a stratocumulus-topped ABL under a subsidence inversion in the North Sea during the KONTROL experiment are summarized as follows:

A conventional "dry" Richardson number formulation of the eddy diffusivity fails to reproduce the observed moist adiabatic lapse rate within the cloud layer and underestimates the evaporation at the surface. Both deficiencies are widely reduced if a "moist" formulation is applied which takes into account the effect of condensation by defining the Richardson number in terms of cloud-conservative variables. Both schemes fail, however, to simulate realistic cloud-top entrainment fluxes because the eddy diffusivity vanishes in the inversion layer due to its dependence on local variables.

With the TKE-scheme, the cloud-top entrainment is simulated more realistically because the turbulence generated by buoyancy within the cloud layer can be transported up and down by turbulent diffusion. The turbulent transport of TKE not only contributes to the maintenance of the well-mixed sub-cloud layer but also to a non-negligible level of turbulence above the cloud layer. The degree of coupling between the cloud layer, the sub-cloud layer and the inversion layer depends crucially on the choice of a parameter which controls the mixing length in stable conditions. Sensitivity experiments with a doubled and halved "entrainment parameter", respectively, indicate that large entrainment of dry and warm air into the ABL promotes not only cloud generat-

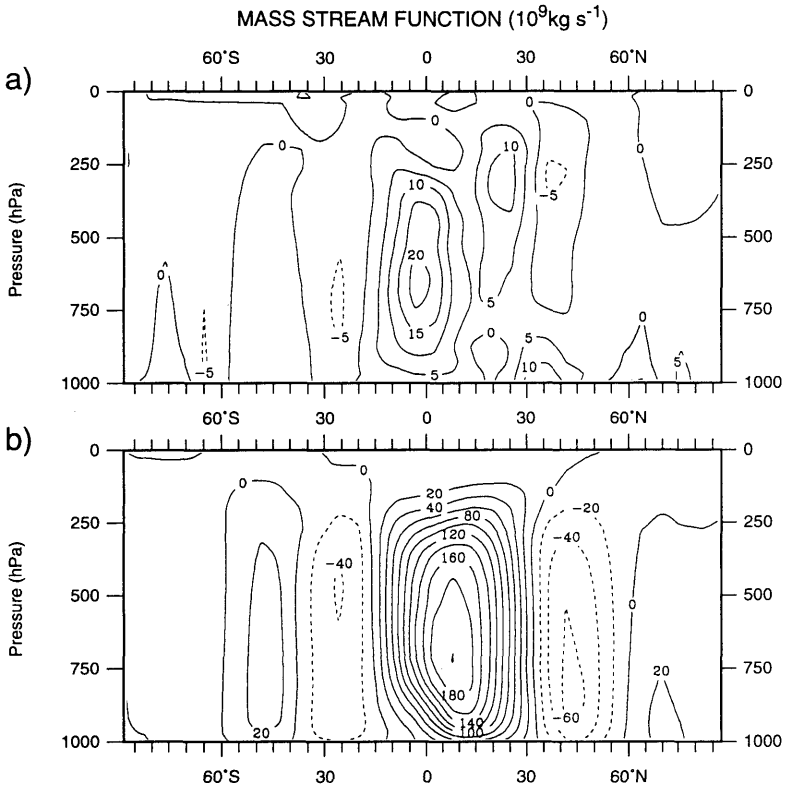

Fig. 13. Latitude-pressure cross sections of the mass stream function. (a) Difference between TKCC and STDR (Contour spacing: $5x10^9$ kg s^{-1}). (b) Experiment TKCC (Contour spacing: $2x10^{10}$ kg s^{-1}).

ing processes, such as additional moisture supply by enhanced surface evaporation, but also cloud dissipating processes such as the evaporation of cloud droplets. In this particular case of a stratocumulus layer under a pronounced subsidence inversion, the net effect of doubling the entrainment parameter is a dilution of the cloud while additional cloud water is generated if the parameter is halved with respect to the control experiment.

Although the processes discussed above can also be identified in the 3d climate simulations, the final result is different. As compared to the standard K-model, the TKE closure enhances the formation of ABL clouds. Moreover, a relatively large entrainment parameter as in the TKDE experiment favours cloud formation through enhanced moisture supply from the surface as a result of an efficient ventilation of the ABL. The surface layer, on the other hand, becomes drier so that the excessive low-level cloudiness simulated by the standard scheme is reduced with the TKE-scheme, particularly in the large-entrainment experiment. The enhanced supply of moisture in all TKE experiments leads to an overall warming and moistening of the troposphere which is related to the extra release of latent heat in stratiform and convective clouds. The hydrological cycle is intensified and the mass transport in the Hadley cell increases as a result of more vigorous tropical convection. Little sensitivity is found with respect to the advective transport of turbulent kinetic energy. Crucially important, however, is the use of cloud-conservative variables in the definition of the buoyancy flux term in the TKE equation.

In conclusion, the results obtained with a set of ABL model formulations suggest that a conventional K-model may not be able to simulate the

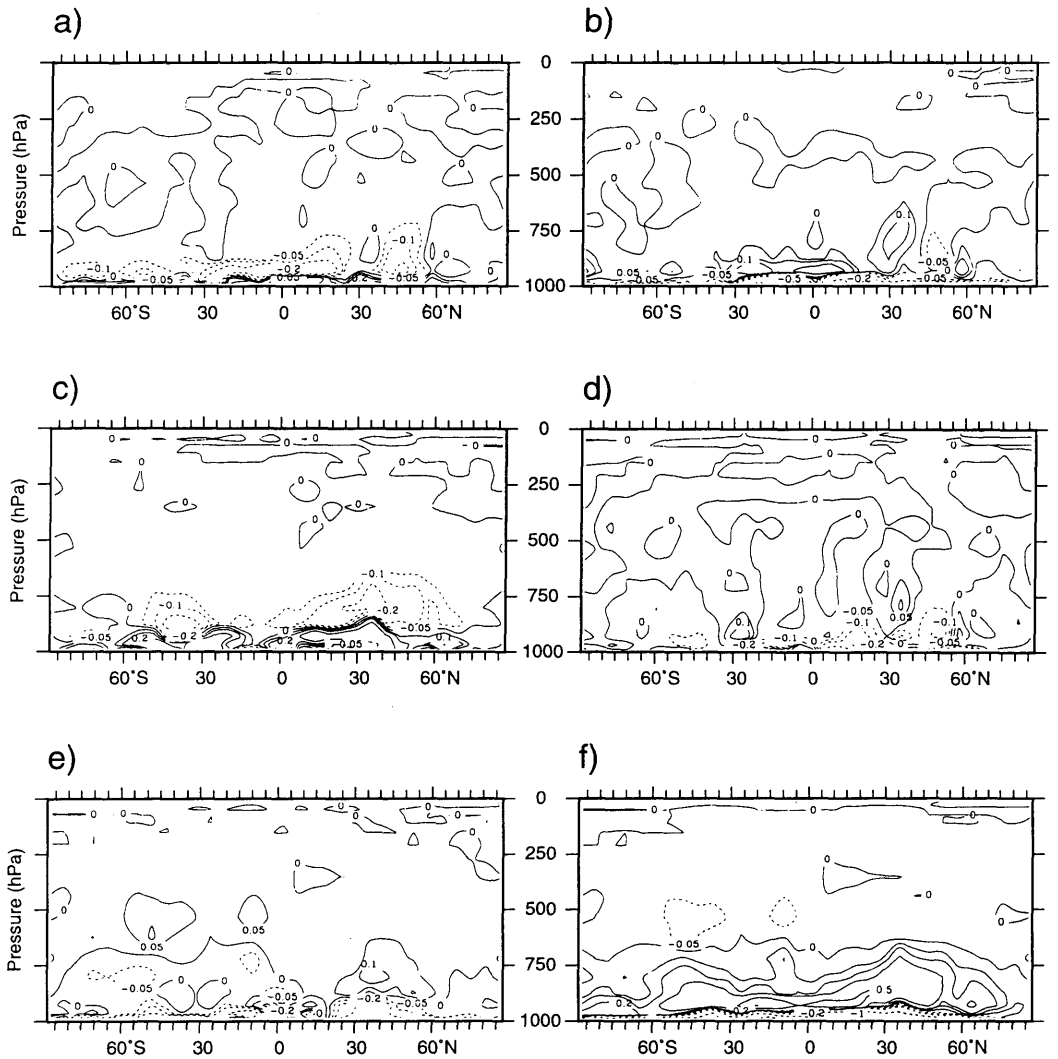

Fig. 14. Sensitivity to model assumptions of the moistening by vertical diffusion of specific humidity. Units: g kg^{-1} d^{-1}. See also Fig. 1. (a) Effect of halved entrainment parameter (TKHE-TKCC). (b) Effect of doubled entrainment parameter (TKDE-TKCC). (c) Effect of a "dry" TKE-closure (TKDR-TKCC). (d) Effect of including TKE advection (TKAD-TKCC). (e) Effect of a "wet" first-order scheme (STCC-STDR). (f) Effect of a higher-order closure (TKCC-STCC). Isolines: $\pm$0, 0.05, 0.1, 0.2, 0.5, 1, 2 (g kg^{-1} d^{-1}).

complex interactions between the cloud-topped ABL and the free troposphere above. A higher-order closure (e.g., the TKE-scheme used in this study) seems more adequate since it allows to represent the cloud-top entrainment resulting from internal TKE sources in the cloud layer in a more realistic manner.

6. Acknowledgements

This research was supported by Deutsche Forschungsgemeinschaft (DFG) through the Sonderforschungsbereich 318 (Klimarelevante Prozesse im System Ozean-Atmosphäre-Kryosphäre) at the University of Hamburg. We would like to thank

our colleagues for valuable comments, and we are grateful to Claudia Schröder for assistance with the manuscript and Norbert Noreiks for drawing the figures.

7. Appendix A

The TKE-eq. (14) is solved by the method of fractional steps. According to the leap-frog time scheme of ECHAM, we use the time levels $(t-1)$ and $(t+1)$.

(1) First, the transport due to advection is determined. Since the wind velocity is defined on the "full" levels of the model (where all prognostic variables are defined), whereas the turbulent kinetic energy is defined on the "half" levels (i.e., between the full levels), the advection term needs to be formulated in a special way. A simple linear interpolation of the TKE to the full levels and back to the half levels after calculation of the advective tendencies results in large truncation errors. Therefore, the wind is interpolated to the half levels instead,

$$\left(\frac{\partial E_{k+1/2}}{\partial t}\right)_{\text{adv}} = \frac{(v_k^i + v_{k+1}^i)}{2} \frac{\partial E_{k+1/2}}{\partial x^i} \tag{A1}$$

and the time derivative is approximated by

$$\left(\frac{\partial E}{\partial t}\right)_{\text{adv}} = \frac{E^{(t+1)*} - E^{(t-1)}}{2\,\Delta t}, \tag{A2}$$

with $(k+\frac{1}{2})$ denoting half levels, $(k+1)$, (k) denoting full levels and i the cartesian coordinates.

(2) Using the new values of $E^{(t+1)*}$ including the advective tendencies, the contribution from buoyancy, shear and dissipation is calculated implicitly in a single equation of the form:

$$\frac{\partial E}{\partial t} = B\sqrt{E} - C\sqrt{E^3} \tag{A3}$$

with

$$B = \frac{g}{\theta_v} l_h c_1 \left[A \frac{\partial \theta_L}{\partial z} + D\theta \frac{\partial q_t}{\partial z} \right] + l_m c_1 \left[\left(\frac{\partial u}{\partial z}\right)^2 + \left(\frac{\partial v}{\partial z}\right)^2 \right], \tag{A4}$$

$$C = \frac{c_1^3}{l_m}. \tag{A5}$$

The finite difference formulation of (A3) gives

$$E^{(t+1)**} = E^{(t+1)*} + (B\sqrt{E^{(t+1)**}} - C\sqrt{(E^{(t+1)**})})\,2\,\Delta t \tag{A6}$$

(3) In the last step, $E^{(t+1)**}$ including advective and source terms is used as initial value to solve the vertical diffusion equation,

$$E^{(t+1)} = E^{(t+1)**} - \frac{\partial}{\partial z}\left(K_m \frac{\partial E^{(t+1)}}{\partial z}\right) 2\,\Delta t. \tag{A7}$$

Eq. (A3) cannot be solved analytically. According to Janjic et al. (1987), it can be modified, however, to describe the time evolution of the square root of the TKE:

$$\frac{\partial \sqrt{E}}{\partial t} = \frac{B}{2} - C\frac{E}{2}. \tag{A8}$$

The corresponding finite difference approximation is

$$\frac{\sqrt{E^{(t+1)}} - \sqrt{E^{(t-1)}}}{2\,\Delta t} = \frac{B}{2} - \frac{C(\sqrt{E^{(t+1)}})^2}{2}. \tag{A9}$$

This is a quadratic equation in $\sqrt{E}$ with the solution:

$$(\sqrt{E^{(t+1)}})_{1,2} = \frac{1}{2\,\Delta t C} \times [-1 \pm \sqrt{1 + C2\,\Delta t(B2\,\Delta t + 2\sqrt{E^{(t-1)}})}]. \tag{A10}$$

Only the first solution has a physical meaning, i.e., $\sqrt{E^{(t+1)}} \to \sqrt{E^{(t-1)}}$ for $\Delta t \to 0$. The critical Richardson number is set to 1 in the model which means that shear production is equal to the destruction of TKE by negative buoyancy. In this case, the term B defined by (A4) vanishes. This assumption garantees that no negative values of E occur under the square root. If the Richardson number is larger than 1, it is assumed that the TKE reaches a background value of 10^{-4} m^2/s.

REFERENCES

Albrecht, B. A., Randall, D. A. and Nicholls, S. 1988. Observations of marine stratocumulus clouds during FIRE. *Bull. Amer. Meteor. Soc.* **69**, 618–626.

Betts, A. K. 1973. Non-precipitating cumulus convection and its parameterization. *Quart. J. Roy. Met. Soc.* **99**, 178–196.

Blackadar, A. K. 1962. The vertical distribution of wind and turbulent exchange in a neutral atmosphere. *J. Geophys. Res.* **67**, 3095–3102.

Brinkop, S. 1991. Inclusion of cloud processes in the ECHAM PBL parameterization. In: *Studying climate with the ECHAM atmospheric model* (ed. R. Sausen). Large-scale atmospheric modelling, Report no. 9, 5–14. Meteorologisches Institut der Universität Hamburg, Germany.

Brinkop, S. 1992. Parameterisierung von Grenzschichtwolken für Zirkulationsmodelle. In: *Berichte aus dem Zentrum für Meeres- und Klimaforschung*, Reihe A: Meteorologie, nr. 2, 77 pp. Meteorologisches Institut der Universität Hamburg, Germany.

Brümmer, B. 1986. KONTROL 1985 Field Phase Report. *Hamburger Geophysikalische Einzelschriften*, Reihe B, Heft 5.

Chen, C. and Cotton, W. R. 1987. The physics of the marine stratocumulus-capped mixed layer. *J. Atmos. Sci.* **44**, 2951–2977.

Clarke, R. H., Dyer, A. J., Brook, R. R., Reid, D. G. and Toup, A. J. 1971. The Wangara Experiment: Boundary-layer data. *Technical Paper no. 19*, 21 pp. Division of Meteorological Physics, CSIRO, Australia.

Deardorff, J. W. 1980. Stratocumulus-capped mixed layers derived from a three-dimensional model. *Bound. Lay. Meteorol.* **18**, 495–527.

Dümenil, L. and Todini, E. 1992. A rainfall-runoff scheme for use in the Hamburg climate model. In: *Advances in theoretical hydrology, a tribute to James Dooge* (ed. J. P. O'Kane). European Geophysical Society Series on Hydrological Sciences, 1, Elsevier Science, Amsterdam, 129–157.

Finger, J. E. and Wendling, P. 1990. Turbulence structure of Arctic stratus clouds derived from measurements and calculations. *J. Atmos. Sci.* **47**, 1351–1373.

Hense, A., Kerschgens, M. and Raschke, E. 1982. An economical method for computing radiative transfer in circulation models. *Quart. J. Roy. Meteor. Soc.* **108**, 231–252.

Janjic, Z., Mesinger F. and Black, T. L. 1987. Horizontal discretization and forcing. *ECMWF Workshop on Techniques for horizontal discretization in numerical weather prediction models*, pp. 207–228, European Centre for Medium Range Weather Forecasts, Reading, UK.

Lilly, D. K. 1968. Models of cloud topped mixed layers under a strong inversion. *Quart. J. R. Met. Soc.* **94**, 292–309.

Louis, J. F. 1979. A parametric model of vertical eddy fluxes in the atmosphere. *Bound. Layer Meteor.* **17**, 187–202.

Mailhot, J. and Benoit, R. 1982. A finite-element model of the atmospheric boundary layer suitable for use with numerical weather prediction models. *J. Atmos. Sci.* **39**, 2249–2266.

Moeng, C. H. 1986. Large eddy simulation of a stratus topped boundary layer. Part I: Structure and budget. *J. Atmos. Sci.* **43**, 2886–2900.

Moeng, C. H. and Schumann, U. 1991. Composite structure of plumes in stratus topped boundary layers. *J. Atmos. Sci.* **48**, 2280–2291.

Nicholls, S. and Leighton, J. 1986. An observational study of the structure of stratiform cloud sheets. Part I: Structure. *Quart. J. Roy. Met. Soc.* **112**, 431–460.

Nicholls, S. and Turton, J. D. 1986. An observational study of the structure of stratiform cloud sheets. Part II: Entrainment. *Quart. J. Roy. Met. Soc.* **112**, 461–480.

Ramanathan, V., Cess, R. D., Harrison, E. F., Minnis, P., Barkstrom, B. R., Ahmad, E., Hartmann, D. 1989. Cloud-radiative forcing and climate: Results from the Earth Radiation Budget Experiment. *Science* **243**, 57–63.

Randall, D. A., Abeles, J. A. and Corsetti, T. G. 1985. Seasonal simulations of the planetary boundary layer and boundary-layer stratocumulus clouds with a general circulation model. *J. Atmos. Sci.* **42**, 641–676.

Roeckner, E., Rieland, M. and Keup, E. 1991. Modelling of cloud and radiation in the ECHAM model. *ECMWF/WCRP Workshop on "clouds, radiative transfer and the hydrological cycle"*, 12–15 November 1990, 199–222, ECMWF, Reading, UK.

Roeckner, E., Arpe, K., Bengtsson, L., Brinkop, S., Dümenil, L., Esch, M., Kirk, E., Lunkeit, F., Ponater, M., Rockel, B., Sausen, R., Schlese, U., Schubert, S. and Windelband, M. 1992. *Simulation of the present-day climate with the ECHAM model: impact of model physics and resolution.* Max-Planck-Institut für Meteorologie, Report no. 93, Hamburg 171 pp.

Rasch, P. J. and Williamson, D. L. 1990. Computational aspects of moisture transport in global models of the atmosphere. *Quart. J. R. Met. Soc.* **116**, 1071–1090.

Smith, R. N. B. 1990. A scheme for predicting layer clouds and their water content in a general circulation model. *Quart. J. R. Met. Soc.* **116**, 435–460.

Stephens, G. L. 1978. Radiation profiles in extended water clouds. Part 2: Parameterization schemes. *J. Atmos. Sci.* **35**, 2123–2132.

Suarez, M. J., Arakawa, A. and Randall, D. A. 1983. Parameterization of the planetary boundary layer in the UCLA general circulation model: Formulation and results. *Mon. Wea. Rev.* **111**, 2224–2243.

Sundqvist, H. 1978. A parameterization scheme for non-

convective condensation including prediction of cloud water content. *Quart. J. R. Met. Soc.* **104**, 677–690.

Tiedtke, M. 1989. A comprehensive mass flux scheme for cumulus parameterization in large-scale models. *Mon. Wea. Rev.* **117**, 1779–1800.

Warren, S. G., Hahn, C. J., London, J., Chervin, R. M. and Jenne, R. L. 1986. *Global distribution of total cloud cover and cloud type amounts over land.* NCAR Tech. Note, NCAR TN-273 + STR, Boulder Colo., and DOE Tech. Rep. ER/60085-H1, 29 pp., 199 maps, US Dept. of Energy, Washington, DC, USA.

Warren, S. G., Hahn, C. J., London, J., Chervin, R. M. and Jenne, R. L. 1988. *Global distribution of total cloud cover and cloud type amounts over the ocean.* NCAR Tech. Note, NCAR TN-317 + STR, Boulder Colo., and DOE Tech. Rep. ER/0406, 42 pp., 170 maps, US Dept. of Energy, Washington, DC, USA.